FACTORS AFFECTING THE OPERATION OF LASER-TRIGGERED GAS SWITCH (LTGS) WITH MULTI-ELECTRODE SPARK GAP

S. J. MacGregor [1ξ], I. V. Timoshkin[1], M. J. Given[1], R. A. Fouracre[1], J. M. Lehr[2] and L. K. Warne[2]

[1]*Institute for Energy and Environment, University of Strathclyde, 204 George St, GlasgowG1 1XW, United Kingdom*

[2]*Sandia National Laboratories, P.O.Box 5800, Albuquerque, NM 87185, USA*

Abstract

Multi-electrode spark switches can be used for switching applications at elevated voltages or for command triggering. Symmetrical field graded electrodes allow the electrical stress across individual gaps to be controlled, thus maximising the hold off voltage and reducing switch pre-fire.

The paper considers some aspects of multielectrode switch design and their influence on switching behavior. Non-symmetrical, uni-directional electrode topologies can be employed with advantages over traditional symmetrical design. The choice of working gas and gas pressure can influence switching performance in terms of delay-time and jitter. Transient analysis of switch characteristics has been undertaken in order to understand multi-electrode switching.

I. INTRODUCTION

Multi-electrode, cascade, gas-filled switches are used in different pulsed power applications. The LTGS Sandia switch is a spark switch with a trigger section and a multi-electrode cascade section that allows voltage grading across the cascade and is designed with 25 MV/m field in the cascade gaps. Laser breakdown of the trigger section causes the fields on the cascade sections to rise significantly above the nominal pre-breakdown value and thus cause switch closure. Modeling of the transients occurring during switch closure can lead to an understanding of the switching process and thus possible improvements in the LTGS design and operation.

II. POTENTIAL IMPROVEMENTS TO SWITCH DESIGN

The energy of the laser pulse dissipated in the gas filled trigger initiates the spark breakdown in that section. However, the resultant breakdown of the cascade section can be caused by several mechanisms. The discharge could be triggered by energetic electrons produced in the gas either by field ionization resulting from overvolting or by environmental UV photons originating from the discharge in the trigger section or from local partial flashovers in the cascade section. Alternatively, an electron avalanche can be caused by field emission from the cascade electrodes which can occur for electric fields above 10-20 MV/m [1]. It must therefore be considered as a possible mechanism of discharge initiation.

On the other hand, the statistics of field-induced, electron emission may be such that the cascade gaps are virtually inactive until laser gap closure, at which point the enhanced field causes spontaneous electron emission from the cascade electrodes leading to breakdown. Field emission should be controlled to ensure better switch performance along with minimization of UV photon production by shielding of critical high-field areas.

A. Non-symmetrical electrode topologies

If the initiatory electron production does occur through field emission then there is no advantage in using symmetrical cascade electrodes. Non-symmetrical floating "toroidal" electrodes as shown in Figure 1 will reduce the field enhancement at the negative electrode and thus reduce field emission. This approach may allow the performance of the cascade section to be improved.

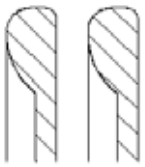

Figure 1. Conceptual design of the uni-directional cascade electrodes.

It was shown experimentally by MacGregor *et al.* [2] that the breakdown voltage for a system with a protrusion on a flat electrode surface behaves differently for negative and positive pulses. When the protrusion is positively biased the breakdown voltage is higher. Thus it is to be expected

[ξ] email: sjm@eee.strath.ac.uk

that non-symmetrical electrodes could withstand higher voltages without breakdown.

B. Leader transition effects, gas mixtures, dielectric coating

Better understanding of the leader-streamer transition in a non-uniform field could result in improvements in the design and operation of the cascade switch. In SF_6 the breakdown characteristics of non-uniform gaps is determined by the formation and propagation of leaders. The conditions necessary for leader propagation are not yet fully understood. It has been shown that the gas pressures at which a transition from a streamer to a leader occurs in SF_6-air mixtures increase as more air (18% or 36%) is added [3]. This suggests that the use of gas mixtures could improve the cascade switch performance. Although adding 18% or 36% of air to SF_6 reduces the breakdown voltage at lower pressures, as the pressure is increased the breakdown voltage continues to rise smoothly rather than saturating or collapsing. Thus at higher pressures of SF_6 mixtures higher breakdown voltages can be achieved thus potentially improving switch performance.

III. MODELING OF THE SWITCH PERFORMANCE

The above mechanisms are strongly voltage dependant. Therefore a knowledge of the magnitude and duration of the transient voltages to which the switch is subjected during operation is required prior to considering further the precise mechanism of switch operation.

The multi-stage switch consists of a laser triggering section, a cascade section with 26 toroidal symmetrical electrodes and is attached to an intermediate storage capacitor (ISC). These have been modeled using a simple lumped, equivalent electric circuit. The capacitance of the laser triggering section is modeled by a capacitor C_3, the cascade section by capacitance C_2. Capacitor C_1 represents both the intermediate energy store and the external stray capacitance of the switch.

The cascade section has 25 identical electrode gaps which grade the voltage capacitevly across the switch. The capacitance of each individual gap has been estimated using "ELECTRO", 2D electrostatic software which provides capability of 3D modeling of rotationally symmetrical objects. Geometrical models of the electrodes have been created in "ELECTRO" and the electrical charge, Q, on the electrodes has been obtained. The capacitance of the gap has been calculated as $C=Q/V$, where V is the applied voltage. Using this approach it has been shown that each individual inter-electrode gap has a capacitance of about 20 pF which gives a total capacitance value for the cascade section C_2=0.8 pF. The estimated capacitance of the laser triggered section is C_3=6.2 pF. The value of the stray capacitance of the switch was taken from reference [4] and this value is 17 pF. The capacitance of the intermediate storage capacitor (ISC) is 24 nF. Because the stray capacitance of the switch and the ISC capacitance are parallel capacitances, the value of C_1 can be taken as 24 nF, in the case when the ISC is included in the analysis of the transient process. As a limiting case, the transient process has also been considered for the model circuit excluding the ISC capacitance, and in this situation C_1=17 pF.

A. Breakdown of the laser- triggered gap

A schematic diagram of the LTGS switch is shown in Figure 2. Application of a laser pulse results in gas breakdown of the triggered gap. Consequently the parameters for the resulting transient plasma channel have to be included in the equivalent circuit. These have been assigned the following values: inductance L=150 nH, and resistance R=0.2 Ohm. Both the inductance and the resistance were considered to be constant in order to simplify analytical calculations. In the figure, voltage sources V_{CAS-0}, V_{03}, V_{01}, represent respectively the initial voltages across the cascade, the laser triggered section and the complete switch prior to breakdown of the laser triggered gap.

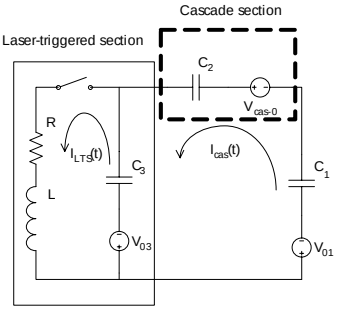

Figure 2. Schematic model of the cascade switch before the cascade section breakdown. RLC_3 loop models the plasma channel in the laser triggered section.

Upon closure of the laser-triggered section, transient currents flow as shown in Figure 1 due to the rearrangement of the charge distribution on the capacitances C_1, C_2 and C_3.

The differential equations governing the above circuit in the Laplace s-domain are:

$$\begin{aligned} I_{LTS} z_{11} - I_{CAS} z_{12} &= -V_{03} s^{-1} \\ I_{CAS} z_{22} - I_{LTS} z_{12} &= (V_{03} + V_{02} - V_{01}) s^{-1} \end{aligned} \quad (1)$$

where

$$z_{11} = Ls + R + C_3^{-1} s^{-1};\ z_{22} = \left(C_1^{-1} + C_2^{-1} + C_3^{-1}\right) s^{-1};\ z_{12} = C_3^{-1} s^{-1}$$

Solution of these equations result in analytical time-domain expressions for the currents in the cascade section, $I_{CAS}(t)$ and in the laser triggered section, $I_{LTS}(t)$ as given by equations (2) below.

$$I_{CAS}(t) = GV_{03}\exp\left\{-\frac{t}{\tau_0}\right\}\sin(\omega t),\ I_{LTS}(t) = \frac{C_3}{C^*}I_{CAS}(t) \quad (2)$$

where

$$G = \frac{C^*}{C_3}\frac{1}{\omega L},\ \tau_0 = \frac{2L}{R},\ \omega = \sqrt{\frac{1-C^*/C_3}{LC_3} - \frac{1}{\tau_0^2}},\ \frac{1}{C^*} = \frac{1}{C_1} + \frac{1}{C_2} + \frac{1}{C_3}$$

The magnitude of the transient voltage across the cascade section, $V_{cas}(t)$, can be derived using the expression for the current, $I_{CAS}(t)$:

$$V_{CAS}(t) = \frac{1}{C_2}\int GV_{03}\exp\left\{-\frac{t}{\tau_0}\right\}\sin(\omega t)dt + V_{cas-0} \quad (4)$$

After integration of (4) the final expression for the magnitude of the voltage drop across the cascade is:

$$V_{CAS}(t) = \frac{GV_{03}}{C_2}\frac{1}{\tau_0^{-2}+\omega^2}\times \left[\exp\left\{-\frac{t}{\tau_0}\right\}\times\left\{\frac{1}{\tau_0}\sin(\omega t)+\omega\cos(\omega t)\right\}-\omega\right] + V_{CAS-0} \quad (5)$$

Figure 2 shows the dynamics of the normalized transient voltage, $V_{cas}(t)/V_{cas-0}$, across the cascade section after closure of the laser-triggered gap by a plasma channel. The solid line shows the transient normalized voltage when the ISC is included in the circuit analysis, that is when C_1=24 nF , and the dashed line shows the transient process for the circuit without inclusion of the ISC, when C_1 represents only the stray capacitance of the switch, that is C_1=17 pF.

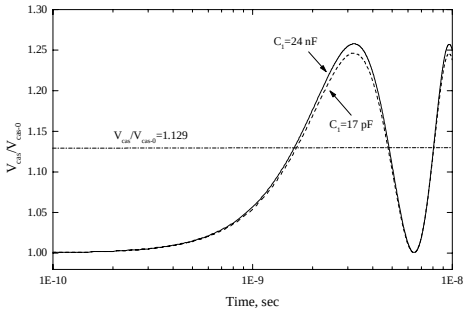

Figure 2. Normalized transient voltage across the cascade section after the spark closure of the laser triggered gap.

It can be seen that when ISC is included the voltage reaches its maximum of $1.258V_{CAS-0}$ at 3.2 ns. It then oscillates with an angular velocity of ω=9.78·10^8 rad/sec, and has a relatively long decay constant of τ_0=1.5 μs. If the ISC is not included the maximum normalized voltage is fractionally decreased but the angular velocity remains the same.

The dash-dotted horizontal line in Figure 2 shows the normalized voltage across the cascade after the end of the transient process in the circuit with the ISC incorporated. This voltage can be calculated using the static capacitive model based on the charge conservation law. The charge stored on the laser trigger gap capacitance C_3 is re-distributed between the cascade section C_2 and the ISC capacitance C_1 due to plasma shorting of the trigger gap. Hence, after the transient process in the laser-triggered gap has ceased the switch can be modeled by two parallel capacitors: C_1 and C_2. Using this approach, the normalized voltage across the cascade can be written as:

$$\left.\frac{V_{CAS}}{V_{CAS-0}}\right|_{t>>\tau_0} = \frac{C_1(1+C_2/C_3)+C_2}{C_1+C_2} \quad (6)$$

The value of the normalized voltage across the cascade section for long times given by the analytical solution and that by considering charge redistribution are identical.

B. Breakdown of the cascade gap

After closure of the laser-triggered spark gap it is assumed that a single gap in the cascade breaks down. This second transient process can be modeled by including in the lumped circuit representing the switch assembly an additional inductance and resistance associated with the cascade gap plasma channel. The single cascade gap capacitance is C_{S1}, and the capacitance of the remaining 24 gaps is C_{21}. The modified circuit is shown in Figure 3. Voltage sources V_{0s1}, V_{021}, V_{031}, V_{011}, represent respectively the initial voltages across the single cascade gap, the remaining cascade, the laser triggered section and the complete switch prior to the breakdown event. The voltage source, LI_{01}, models the voltage drop across the spark channel inductance in the laser-triggered section at the time of the cascade gap breakdown.

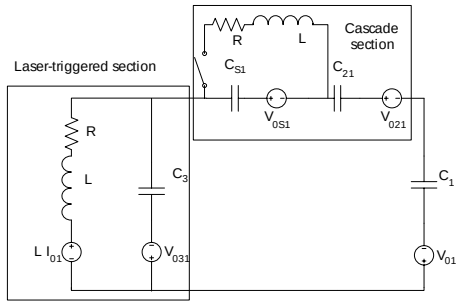

Figure 3. The circuit diagram model of the transient process in the switch after the closure of the laser triggered gap. The RLC_{s1} loop models the transient current in the first cascade gap.

To solve this problem analytically two simplifications have been introduced. First, the capacitance of the laser triggered section has been taken to be equal to the

capacitance of an individual cascade gap, so that C_3=C_{s1}= 20 pF. Second, the term

$$\frac{2C^{**}}{C_3} \approx 0.107 \text{, where } \frac{1}{C^{**}} = \frac{1}{C_1} + \frac{1}{C_{21}} + \frac{1}{C_3} \qquad (7)$$

can be considered as much smaller than unity and under certain circumstances can be neglected. Using these simplifications, it is possible to obtain an analytical form for the transient current in the unbroken cascade section, $I_{CAS\text{-}1}(t)$. It is assumed that the breakdown of the first cascade gap occurs at the first maximum of the transient voltage across the cascade after closure of the laser-triggered section. Thus the initial conditions for the solution pertaining to the circuit diagram shown in Figure 3 have been taken to be those occurring at the moment of the first voltage peak shown in Figure 2. The analytical solution, derived by a similar approach to that previously used above, is given by:

$$I_{CAS-1}(t) = I_{01}\frac{C^{**}}{C_3}\exp\left\{-\frac{t}{\tau_1}\right\}\left[K\sin(\omega_1 t) + \cos(\omega_1 t)\right] \qquad (8)$$

where

$$K = \frac{(V_{031} + V_{0s1})/LI_{01} - 1/\tau_1}{\omega_1} \qquad (9)$$

The magnitude of the voltage across the remaining cascade section is:

$$V_{CAS-1}(t) = I_{01}\frac{C^{**}}{C_2 C_3}\frac{1}{\tau_1^{-2} + \omega_1^2} \times \left[\exp\left\{-\frac{t}{\tau_1}\right\}\left\{\left(\omega_1 - \frac{K}{\tau_1}\right)\sin(\omega_1 t) + \frac{V_{031} + V_{0s1}}{LI_{01}}\cos(\omega_1 t)\right\} + \frac{V_{031} + V_{0s1}}{LI_{01}}\right] + V_{021}$$

The normalized transient voltage across the cascade section, $V_{cas\text{-}1}(t)/V_{021}$, after the closure of both the laser triggered gap and the first cascade gap is shown in Figure 5. The solid line shows the normalized transient voltage when ISC is included in the circuit analysis, i.e. C_1=24 nF, and the dashed line shows the transient process for the circuit without ISC, in which C_1=17 pF represents the stray capacitance of the switch. In the former case the voltage reaches its maximum of $1.154V_{021}$=$1.452V_{CAS\text{-}0}$ in 5.4 ns after the closure of the cascade gap, then oscillates with an angular velocity of ω=$5.77\cdot10^8$ rad/sec, and has a decay constant of τ_0=1.5 μs. The behavior in the case when ISC is not included in the circuit is similar but the peak voltage is fractionally reduced. The dash-dotted horizontal line in Figure 4 shows the level of the normalized voltage across the cascade after the end of the transient process in the circuit with ISC present.

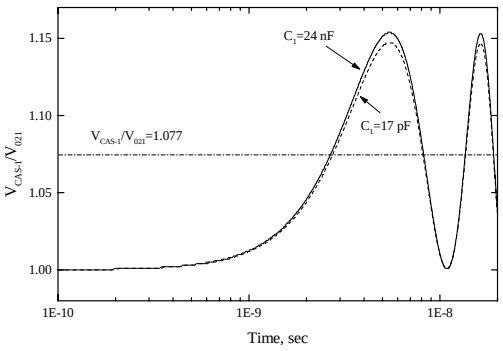

Figure 4. Normalized transient voltage across the cascade section after the spark closure of the first cascade gap.

III. SUMMARY

Several potential improvements in multi-electrode switch design have been considered in the present paper. They include non-symmetrical electrode topologies, use of gas mixtures and effects of streamer to leader transition controlled using gas mixtures. Such improvements may aid achievement of sequential breakdown of the cascade gap and reduction in the switch jitter. The lumped circuit analysis presented shows that the cascade section experiences over-voltage after spark breakdown of each section/gap of the multi-electrode switch. The over-voltage after breakdown of the first cascade gap can be as high as 45% of the initial cascade voltage. It takes a few nanoseconds for the transient voltage to reach its maximum indicating with a high degree of probability that the cascade sections breakdown on the first rising slope of the transient voltage.

IV. REFERENCES

[1] R. Latham, K. Bayliss, and B. Cox, "Spatially correlated breakdown events initiated by field electron emission in vacuum and high pressure SF_6", J. Phys. D: Appl. Phys., vol.19, pp.219-231, 1986.

[2] S. MacGregor, S. Turnbull, F. Tuema, and O. Farish, "Enhanced spark gap switch recovery using nonlinear V/p curves", IEEE Trans. Plasma Sci., vol.32, pp.260-266, 1995.

[3] S. MacGregor, O. Farish, and I. Chalmers, "The switching properties of SF_6 gas mixtures", in Proc. IEEE 7th Int Pulsed power Conf., Monterey, CA, 1989, pp.510-513.

[4] M. Kemp, "Simulation and experimental study of the multichanneling Rimfire gas switch", MSc Thesis, University of Missouri-Columbia, 2005.